

picoline adducts only. This could indicate that as in the case of the Fe^{III} complex, there is a $\nu(\text{M}-\text{N})$ band close to 250 cm^{-1} , overlaid by the strong and broad band 17a. What is clear, however, is that in at least three of the complexes studied here there are at least two infrared-active $\text{M}-\text{N}$ stretches, and this includes the mixed-valence iron(III,III,II) complexes: again confirming that the symmetry is lower than D_{3h} .

There are several indications that although the symmetry of the mixed-valence iron complexes is consistent with unequal oxidation states, the localization of charges is not so clear-cut as in the mixed-metal species. As shown in Figure 8 the frequencies of the two components of ν_{as} ($\text{Fe}^{\text{III}}_2\text{Fe}^{\text{II}}\text{O}$) are out of line with the other complexes, the higher-frequency component being significantly low and the lower frequency component significantly high. Also, the actual bands are broader and less intense in the iron(II) complexes than in the others (Figure 3), and both of these anomalies are greater for the pyridine adduct than for the aquo adduct. Evidently there is some delocalization of the valences, and as pointed out above, this could be either static, or dynamic, or both. From a comparison of electronic spectra and electrochemical data, it has already been argued that static delocalization does occur, and more so in the pyridine than in the aquo adduct.³⁵

(35) Cannon, R. D.; Montri, L.; Brown, D. B.; Marshall, K. M.; Elliott, C. M. *J. Am. Chem. Soc.* **1984**, *106*, 2591.

This would affect the infrared spectra by lessening the difference between $\text{Fe}^{\text{III}}-\text{O}$ and $\text{Fe}^{\text{II}}-\text{O}$ stretching force constants. Dynamic delocalization has also been proposed on the basis of Mössbauer line broadening measurements.^{6,7,24,36} The Mössbauer time scale is much slower than the infrared, but the most recent estimate of k_{et} , for the complex with $L = 4$ -ethylpyridine, extrapolated to room temperature, is $9 \times 10^9\text{ s}^{-1}$.⁶ The half-widths of our observed bands 10a and 10b are approximately 10 cm^{-1} , or in terms of frequency about 10^{11} s^{-1} . The possibility of lifetime broadening through the electron transfer reaction 1 cannot therefore be ruled out.

Acknowledgment. We thank Dr. A. B. Blake for samples of mixed-metal complexes and Dr. D. B. Powell for advice and discussion. L.M. thanks the University of East Anglia and the CVCP for financial support.

(36) (a) Gol'danskii, V. I.; Alekseev, V. P.; Stukan, R. A.; Turtã, K. I.; Ablov, A. V. *Dokl. Akad. Nauk SSSR* **1973**, *213*, 867; *Dokl. Phys. Chem.* **1973**, *213*, 1063; (b) *Fiz. Mat. Metody Koord. Khim., Tezisy Dokl., Vses. Soveshch. 5th* **1974**, 127. Shtiintsa, Kishinev, USSR, 1974; CA 83 35258f. (37) Wilmschurst, J. K.; Bernstein, H. J. *Can. J. Chem.* **1957**, *35*, 1183. (38) Green, J. H. S.; Kynaston, W.; Paisley, H. M. *Spectrochim. Acta* **1963**, *19*, 549. (39) Long, D. A.; George, W. O. *Spectrochim. Acta* **1963**, *19*, 1777.

The Anisotropy of Intermolecular Interactions, Band Electronic Structure, and Electrical Properties of $\beta\text{-(ET)}_2\text{AuCl}_2$

T. J. Emge,[†] H. H. Wang,[†] M. K. Bowman,[†] C. M. Pipan,[†] K. D. Carlson,[†] M. A. Beno,[†] L. N. Hall,[†] B. A. Anderson,[†] J. M. Williams,^{*,†} and M.-H. Whangbo^{*,†}

Contribution from the Chemistry and Materials Science Divisions, Argonne National Laboratory, Argonne, Illinois 60439, and Department of Chemistry, North Carolina State University, Raleigh, North Carolina 27695-8204. Received September 9, 1986

Abstract: A new organic salt, $\beta\text{-(ET)}_2\text{AuCl}_2$, was synthesized, and its structure and physical properties were determined. Here ET refers to bis(ethylenedithio)tetrathiafulvalene (BEDT-TTF or ET). $\beta\text{-(ET)}_2\text{AuCl}_2$ is isostructural with $\beta\text{-(ET)}_2\text{ICl}_2$ and contains the shortest anion, AuCl_2^- , among the $\beta\text{-(ET)}_2\text{X}$ salts with linear anions, X^- , known so far. Crystal data for $\beta\text{-(ET)}_2\text{AuCl}_2$ are as follows: triclinic, $P\bar{1}$, 298 K/120 K, $a = 6.651(1)/6.627(2)\text{ \AA}$, $b = 9.761(2)/9.595(3)\text{ \AA}$, $c = 12.734(3)/12.662(4)\text{ \AA}$, $\alpha = 86.12(2)/85.15(2)^\circ$, $\beta = 100.70(2)/101.40(2)^\circ$, $\gamma = 99.41(2)/98.24(2)^\circ$, and $V_c = 800.7(4)/779.8(5)\text{ \AA}^3$. The electrical conductivities of type I $\beta\text{-(ET)}_2\text{X}$ salts (i.e., those with short anions $\text{X}^- = \text{AuCl}_2^-, \text{ICl}_2^-$) measured by the four-probe technique show that they are semiconductors with thermal activation energy of 0.10 eV. The valence band (i.e., the highest occupied band) of $\beta\text{-(ET)}_2\text{AuCl}_2$, which is half-filled, is calculated to be one-dimensional in character as in the case of $\beta\text{-(ET)}_2\text{ICl}_2$. ESR data of $\beta\text{-(ET)}_2\text{AuCl}_2$ reveal the presence of a phase transition at $\sim 33\text{ K}$, which is somewhat higher than the corresponding temperature (22 K) of $\beta\text{-(ET)}_2\text{ICl}_2$. The ET molecule pairs of type I $\beta\text{-(ET)}_2\text{X}$ salts are significantly more dimerized than those of type II $\beta\text{-(ET)}_2\text{X}$ salts (i.e., those with long anions $\text{X}^- = \text{IBr}_2^-, \text{AuI}_2^-, \text{I}_3^-$). Short S...S contacts within the ET molecule networks of both type I and type II $\beta\text{-(ET)}_2\text{X}$ salts are found to decrease as the length of the anion X^- decreases. This originates from close-packing of ET molecules around the anions X^- in the $\beta\text{-(ET)}_2\text{X}$ salts. For type I $\beta\text{-(ET)}_2\text{X}$ salts with small anions X^- , this close-packing is achieved when dimerized ET molecule pairs protrude out of their donor networks.

For the isostructural $\beta\text{-(ET)}_2\text{X}$ series of synthetic metals and superconductors, where X^- is a linear triatomic anion such as I_3^- ,¹⁻³ I_2Br^- ,^{4,5} AuI_2^- ,^{6,7} IBr_2^- ,^{8,9} or ICl_2^- ,¹⁰ correlations between anion length and the physical properties of their salts have been developed.^{5,10-12} Band electronic structure calculations^{13,14} on $\beta\text{-(ET)}_2\text{X}$ synthetic metals show that their electrical properties are directly related to the magnitudes of donor-donor interactions within the layered networks of ET molecules. Depending on the nature of donor-donor interactions, the ET molecule layer exhibits either a two-dimensional^{13,14} (2D) or a quasi-one-dimensional¹⁰ (1D) electronic behavior. For linear anions, the intermolecular

S...S contacts within the 2D ET networks of the isostructural $\beta\text{-(ET)}_2\text{X}$ salts generally expand as the anion length is increased.^{5,11}

* Authors to whom correspondence should be addressed.

[†] Argonne National Laboratory.

[†] North Carolina State University.

(1) Yagubskii, E. B.; Shchegolev, I. F.; Laukhin, V. N.; Kononovich, P. A.; Kartsovnik, M. V.; Zvarykina, A. V.; Buravov, L. I. *JETP Lett.* **1984**, *39*, 12.

(2) Crabtree, G. W.; Carlson, K. D.; Hall, L. N.; Copps, P. T.; Wang, H. H.; Emge, T. J.; Beno, M. A.; Williams, J. M. *Phys. Rev. B: Condens. Matter* **1984**, *30*, 2958.

(3) Williams, J. M.; Emge, T. J.; Wang, H. H.; Beno, M. A.; Copps, P. T.; Hall, L. N.; Carlson, K. D.; Crabtree, G. W. *Inorg. Chem.* **1984**, *23*, 2558.

(4) Emge, T. J.; Wang, H. H.; Beno, M. A.; Leung, P. C. W.; Firestone, M. A.; Jenkins, H. C.; Cook, J. D.; Carlson, K. D.; Williams, J. M.; Venturini, E. L.; Azevedo, L. J.; Schirber, J. E. *Inorg. Chem.* **1985**, *24*, 1736.

(5) Emge, T. J.; Leung, P. C. W.; Beno, M. A.; Wang, H. H.; Firestone, M. A.; Webb, K. S.; Carlson, K. D.; Williams, J. M.; Venturini, E. L.; Azevedo, L. J.; Schirber, J. E. *Mol. Cryst. Liq. Cryst.* **1986**, *132*, 363.

but no direct correlation between the S...S contacts and the length of the anion has been previously given.

The presence of several S...S contacts shorter than the van der Waals radii sum¹⁵ (~3.60 Å) within the ET molecule network may imply the presence of significant covalent interactions between ET molecules. However, donor-donor interactions in β -(ET)₂X salts are essentially *nonbonding* (slightly antibonding) since the overlap populations calculated for those short S...S contacts are all slightly negative numbers (in the second decimal place).¹⁶ Thus, the most important intermolecular interactions for crystal cohesion in β -(ET)₂X salts are likely of the *donor-anion* type. Low-temperature neutron and X-ray data show the presence of a number of short contacts between the ethylene hydrogen atoms of the ET molecules and anions (i.e., C—H...X⁻ contacts),¹⁷ which result from attractive Coulombic interactions of oxidized ET molecule layers with anion, X⁻ layers. Thus each anion, X⁻, is surrounded in a hydrogen pocket made up of the ethylene groups of ET molecules so that the donor-anion interactions may be described as if effectively weak "H-bonding" exists between the ethylene group hydrogen atoms of the ET molecules and the terminal halide atoms of the linear anions. Although the geometries of these donor-anion interactions are similar, there are two distinct stacking patterns for the ET molecules in β -(ET)₂X salts depending upon the anion length. For the type I β -(ET)₂X salts,¹⁰ namely those with short X⁻ anions, i.e., ICl₂⁻ (8.7 Å), the stacks of ET molecules are greatly dimerized and there are strong pairwise interactions between ET molecules along only one direction, which leads to a one-dimensional (1D) band electronic structure.¹⁰ In contrast, the ET molecules of the type II β -(ET)₂X salts with long X⁻ anions, i.e., I₃⁻ (10.1 Å), I₂Br⁻ (9.7 Å), AuI₂⁻ (9.4 Å), or IBr₂⁻ (9.3 Å), stack with nearly uniform spacings.⁵ As a result, the type II salts have a two-dimensional (2D) band electronic structure, are metallic, and become superconducting at ambient pressure for X⁻ = I₃⁻, AuI₂⁻, and IBr₂⁻.^{13,14,18} In the present work we will show that the β -(ET)₂AuCl₂ salt, recently synthesized by us, represents a new lower limit in anion length (AuCl₂⁻ at 8.1 Å), for a type I β -(ET)₂X salt. In addition, the short interstack S...S distances for all known β -(ET)₂X salts will be correlated with the short C—H...X⁻ distances so as to delineate how the packing of ET molecules in each ET molecule layer is affected by the packing of ET molecules around the anions X⁻.

(6) Wang, H. H.; Beno, M. A.; Geiser, U.; Firestone, M. A.; Webb, K. S.; Nuñez, L.; Crabtree, G. W.; Carlson, K. D.; Williams, J. M.; Azevedo, L. J.; Kwak, J. F.; Schirber, J. E. *Inorg. Chem.* **1985**, *24*, 2465.

(7) Carlson, K. D.; Crabtree, G. W.; Nuñez, L.; Wang, H. H.; Beno, M. A.; Geiser, U.; Firestone, M. A.; Webb, K. S.; Williams, J. M. *Solid State Commun.* **1986**, *57*, 89.

(8) Williams, J. M.; Wang, H. H.; Beno, M. A.; Emge, T. J.; Sowa, L. M.; Copps, P. T.; Behroozi, F.; Hall, L. N.; Carlson, K. D.; Crabtree, G. W. *Inorg. Chem.* **1984**, *23*, 3839.

(9) Carlson, K. D.; Crabtree, G. W.; Hall, L. N.; Behroozi, F.; Copps, P. T.; Sowa, L. M.; Nuñez, L.; Firestone, M. A.; Wang, H. H.; Beno, M. A.; Emge, T. J.; Williams, J. M. *Mol. Cryst. Liq. Cryst.* **1985**, *125*, 159.

(10) Emge, T. J.; Wang, H. H.; Leung, P. C. W.; Rust, P. R.; Cook, J. D.; Jackson, P. L.; Carlson, K. D.; Williams, J. M.; Whangbo, M.-H.; Venturini, E. L.; Schirber, J. E.; Azevedo, L. J.; Ferraro, J. R. *J. Am. Chem. Soc.* **1986**, *108*, 695.

(11) Leung, P. C. W.; Emge, T. J.; Schultz, A. J.; Beno, M. A.; Carlson, K. D.; Wang, H. H.; Firestone, M. A.; Williams, J. M. *Solid State Commun.* **1986**, *57*, 93.

(12) Williams, J. M.; Beno, M. A.; Wang, H. H.; Leung, P. C. W.; Emge, T. J.; Geiser, U.; Carlson, K. D. *Acc. Chem. Res.* **1985**, *18*, 261.

(13) Whangbo, M.-H.; Williams, J. M.; Leung, P. C. W.; Beno, M. A.; Emge, T. J.; Wang, H. H. *Inorg. Chem.* **1985**, *24*, 3500.

(14) Whangbo, M.-H.; Williams, J. M.; Leung, P. C. W.; Beno, M. A.; Emge, T. J.; Wang, H. H.; Carlson, K. D.; Crabtree, G. W. *J. Am. Chem. Soc.* **1985**, *107*, 5815.

(15) Pauling, L. *The Nature of the Chemical Bond*; Cornell University Press: Ithaca, NY, 1960.

(16) Whangbo, M.-H.; Williams, J. M.; Schultz, A. J.; Emge, T. J.; Beno, M. A. *J. Am. Chem. Soc.* **1987**, *109*, 90.

(17) Emge, T. J.; Wang, H. H.; Geiser, U.; Beno, M. A.; Webb, K. S.; Williams, J. M. *J. Am. Chem. Soc.* **1986**, *108*, 3849.

(18) Williams, J. M.; Beno, M. A.; Wang, H. H.; Geiser, U. W.; Emge, T. J.; Leung, P. C. W.; Crabtree, G. W.; Carlson, K. D.; Azevedo, L. J.; Venturini, E. L.; Schirber, J. E.; Kwak, J. F.; Whangbo, M.-H. *Physica* **1986**, *136B*, 371.

Table I. Crystal Data and Structure Refinement Results for β -(ET)₂AuCl₂ at 298 K/120 K

	298 K	120 K
A. Cell Data		
a (Å)	6.651 (1)	6.627 (2)
b (Å)	9.761 (2)	9.595 (3)
c (Å)	12.734 (3)	12.662 (4)
α (deg)	86.12 (2)	85.15 (2)
β (deg)	100.70 (2)	101.40 (2)
γ (deg)	99.41 (2)	98.24 (2)
V (Å ³)	800.7 (4)	779.8 (5)
space group $P\bar{1}$, Z = 1, formula wt = 1037.2, C ₂₀ H ₁₆ S ₁₆ AuCl ₂		
$d_{\text{calcd}} = 2.151$, $d_{\text{meas}} = 2.15$ (1) (neutral buoyancy)		
$\mu = 57.9$ cm ⁻¹ , transmission factors on F _o : 0.36–0.57		
crystal dimensions: 0.42 × 0.20 × 0.10 mm,		
along [100], [010] and [001], respectively		
B. Structural Refinements		
R(F) = $\sum F_o - F_c / \sum F_o $	0.038	0.027
wR(F) = $[\sum w(F_o - F_c)^2 / \sum wF_o^2]^{1/2}$	0.035	0.026 ^a
GOF = $[\sum w(F_o - F_c)^2 / (\text{NO}-\text{NV})]^{1/2}$	1.710	1.388
residuals (e ⁻ /Å ³)	±1.0	±1.4 ^b
NO, no. of observations	3715	6923 ^c
NV, no. of variables	178	178
no. of data collected	4874	7747
2 θ range, (deg), Mo K α (monochromator)	0–55	0–70

^aThe terms minimized in the full-matrix least-squares refinement were $\sum w(|F_o| - |F_c|)^2$, with weights $w = 1/\sigma^2$ and variances $\sigma^2 = \sigma_c^2 + (0.02F_o)^2$, where σ_c are from counting statistics. ^bThe largest residual was in the vicinity of the Au atom; the next largest residual was 0.8/0.7 e/Å³ at 298 K/120 K, respectively. ^c $R_{\text{av}} = \sum ||F_o| - |F_c|| / \sum |F_o|$ = 0.014 at 120 K, with 350 terms having multiple observations. At 298 K, only the 2 standard reflections had multiple observations.

Synthesis of β -(ET)₂AuCl₂

Black needle-like crystals of β -(ET)₂AuCl₂ were prepared by electrocrystallization (Pt electrodes) of 1.9 mM ET and 14.2 mM (*n*-Bu₄N)AuCl₂¹⁹ in 15 mL of tetrahydrofuran at 22 °C and a current density of 1.0 μ A/cm². The solvent was thoroughly degassed, and the cell was assembled inside a drybox. After 1 week of crystal growth, 3.7 mg of product were harvested from the anode (20% yield). On the basis of ESR and X-ray measurements of many samples, only a single phase, β -(ET)₂AuCl₂, was found. This material was later found to be isostructural¹⁰ to β -(ET)₂ICl₂, on the basis of X-ray diffraction data.

X-ray Diffraction Data

The unit cell data and structural refinement results from 298 and 120 K X-ray data are listed in Table I. Intensity data were collected at 298 K on an automated Picker diffractometer and at 120 K on a Syntex P2₁ diffractometer that was equipped with a LN₂-cooled low-temperature device. Each θ -2 θ scan began 1.2° below the Mo K α ₁ diffracted beam and ended 1.3° above the Mo K α ₂, with a constant background/scan time ratio of 1/2. During the course of both data collections, two standard reflections were monitored after every 94 reflections, and no significant variations in their intensities were observed. Corrections for Lorentz effects, polarization, and absorption were applied to all data. Further details of the diffraction experiments are included in Table I. The derived positional and equivalent isotropic thermal parameters at 298 and 120 K for all non-hydrogen atoms of the unique ET molecule and the AuCl₂⁻ anion are given in Table II. The bond distances and angles for the unique ET molecule and anion of β -(ET)₂AuCl₂ are listed in Table III.

Resistivity Measurements

Measurements of the temperature dependence of the electrical resistivity of β -(ET)₂AuCl₂ and for comparison β -(ET)₂ICl₂ were carried out by the use of the 4-probe technique with ac currents and phase-sensitive detection. Currents of ~0.5 μ A at a frequency of ~37 Hz were used. The current and voltage probes consisted

(19) Braunstein, P.; Clark, R. J. H. *J. Chem. Soc., Dalton Trans.* **1973**, 1845.

Table II. Positional and Equivalent Isotropic Thermal Parameters for β -(ET)₂AuCl₂ at 298 K/120 K^a

atom	x	y	z	U_{eq} (Å ²)
Au	0.00000	0.00000	0.00000	0.0454 (2)
	0.00000	0.00000	0.00000	0.0160 (1)
C1	0.09294 (18)	0.21444 (12)	-0.07274 (9)	0.0543 (5)
	0.08525 (7)	0.21765 (5)	-0.07685 (4)	0.0192 (2)
S1	0.41670 (14)	-0.26179 (10)	0.53997 (8)	0.0356 (6)
	0.41319 (6)	-0.26363 (5)	0.54023 (4)	0.0135 (2)
S2	0.02201 (14)	-0.17599 (10)	0.55906 (8)	0.0345 (3)
	0.01483 (7)	-0.17543 (4)	0.55944 (4)	0.0130 (1)
S3	0.17855 (13)	-0.46301 (10)	0.34911 (7)	0.0319 (6)
	0.17631 (6)	-0.46352 (4)	0.34889 (3)	0.0123 (2)
S4	-0.21598 (14)	-0.37980 (10)	0.37100 (8)	0.0355 (6)
	-0.22286 (6)	-0.37833 (5)	0.36959 (4)	0.0134 (2)
S5	0.66834 (16)	-0.07991 (13)	0.70870 (10)	0.0448 (5)
	0.66592 (7)	-0.08236 (5)	0.70982 (4)	0.0160 (3)
S6	0.19514 (16)	0.01137 (11)	0.73579 (10)	0.0419 (4)
	0.18721 (7)	0.00998 (5)	0.73813 (4)	0.0161 (1)
S7	0.00638 (15)	-0.63103 (11)	0.15916 (8)	0.0386 (7)
	0.00392 (7)	-0.63310 (5)	0.15880 (4)	0.0140 (2)
S8	-0.46603 (14)	0.53016 (11)	0.18917 (8)	0.0394 (4)
	-0.47375 (7)	-0.52913 (5)	0.18787 (4)	0.0147 (1)
C1	0.1506 (5)	-0.2786 (4)	0.4955 (3)	0.0306 (22)
	0.1454 (2)	-0.2793 (2)	0.4961 (1)	0.0130 (8)
C2	0.0497 (5)	-0.3644 (4)	0.4156 (3)	0.0307 (22)
	0.0445 (2)	-0.3640 (2)	0.4153 (1)	0.0121 (8)
C3	0.4242 (6)	-0.1406 (4)	0.6364 (3)	0.0324 (14)
	0.4201 (3)	-0.1439 (2)	0.6379 (1)	0.0123 (5)
C4	0.2434 (6)	-0.1031 (4)	0.6468 (3)	0.0313 (14)
	0.2363 (3)	0.1044 (2)	0.6487 (1)	0.0118 (8)
C5	-0.0398 (5)	-0.5252 (4)	0.2554 (3)	0.0321 (23)
	-0.0426 (2)	-0.5268 (2)	0.2549 (1)	0.0107 (5)
C6	-0.2203 (5)	-0.4874 (4)	0.2658 (3)	0.0300 (22)
	-0.2260 (2)	-0.4876 (2)	0.2650 (1)	0.0118 (8)
C7	0.6192 (7)	0.0895 (4)	0.7373 (4)	0.0408 (18)
	0.6113 (3)	0.0897 (2)	0.7373 (2)	0.0155 (6)
C8	0.4533 (7)	0.0823 (5)	0.8029 (4)	0.0437 (18)
	0.4469 (3)	0.0793 (2)	0.8062 (2)	0.0162 (6)
C9	-0.2285 (8)	-0.6262 (6)	0.0616 (4)	0.0564 (23)
	0.2299 (3)	-0.6198 (2)	0.0585 (1)	0.0168 (6)
C10	-0.4224 (7)	-0.6591 (6)	0.1050 (4)	0.0521 (22)
	-0.4270 (3)	-0.6606 (2)	0.1040 (2)	0.0153 (5)

^a Estimated standard deviations are enclosed in parentheses. The equivalent isotropic thermal parameter, U_{eq} , is $1/3 \sum_i \sum_j a_i a_j a_i^* a_j^* U_{ij}$. The temperature factor expression is $\exp[-2\pi^2(U_{11}h_1^2 a^{*2} + U_{22}k_2^2 b^{*2} + U_{33}l_2^2 c^{*2} + U_{12}h_1 k_1 a^* b^* + U_{13}h_1 l_1 a^* c^* + U_{23}k_1 l_1 b^* c^*)]$.

of gold wires attached to the crystals with gold conducting paste along the needle axis (*a* axis). The measurements were carried out on two different crystals of each salt, and the results were comparable and reproducible on the thermal cycling of each specimen. The normalized resistivities are illustrated in Figure 1, A and B. These figures show semiconducting electrical resistivity from 300 K down to ~160 K, which is the lowest temperature at which we could measure the resistance. The resistance remained high, but unmeasurable, down to liquid He temperatures.

The temperature dependence of the resistivities over the measurable range of temperatures precisely follows an exponential law with thermal activation energies of 0.10 eV for both salts. The room temperature resistivities (ρ) were estimated from the slightly irregular crystal dimensions and voltage probe distances to be ~100 Ω cm for β -(ET)₂AuCl₂ and ~300 Ω cm for β -(ET)₂ICl₂.

ESR Measurements

The electron spin resonance (ESR) data were obtained with a single crystal (1.84 × 0.15 × 0.06 mm) of β -(ET)₂AuCl₂ and were recorded by use of a Varian E-9 spectrometer at 9.14 GHz with 100 KHz field modulation and a helium gas flow refrigerator. Figure 2 illustrates the relative spin susceptibility (all values are normalized to the 298 K susceptibility) and peak-to-peak derivative ESR line widths (ΔH_{p-p}) that were measured from 26 to 298 K with the static magnetic field approximately parallel to the crystallographic *c** axis (crystal plate normal). The value of ΔH_{p-p} was 6.2 Oe at 298 K and decreased approximately linearly with

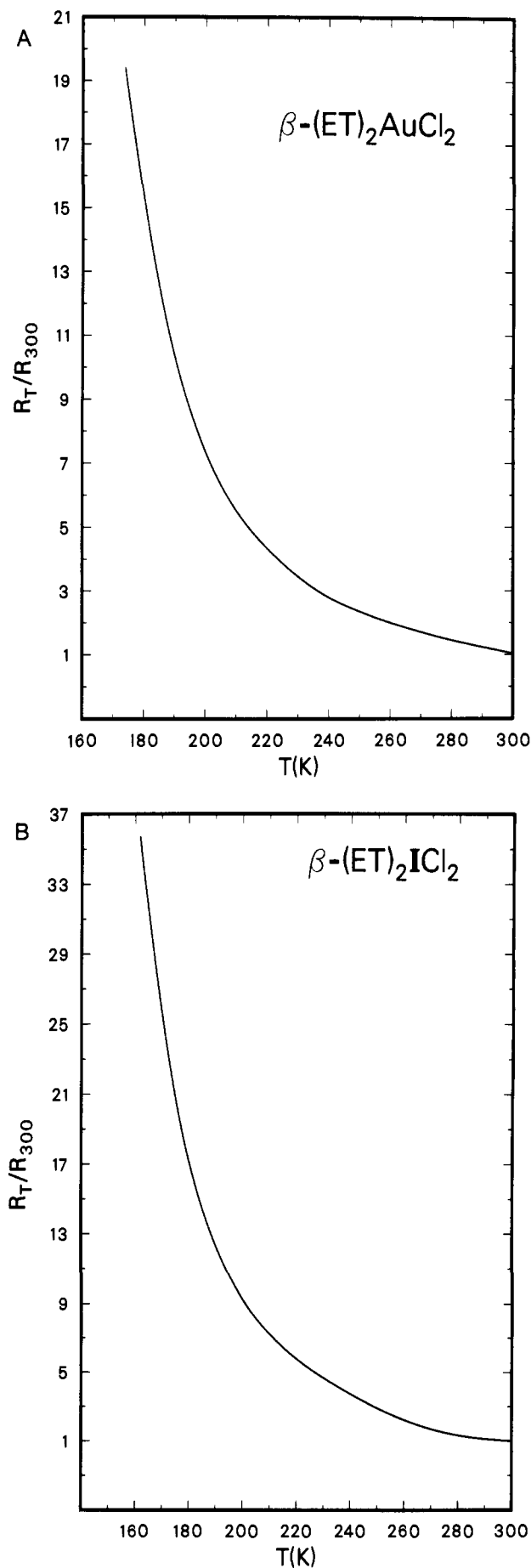
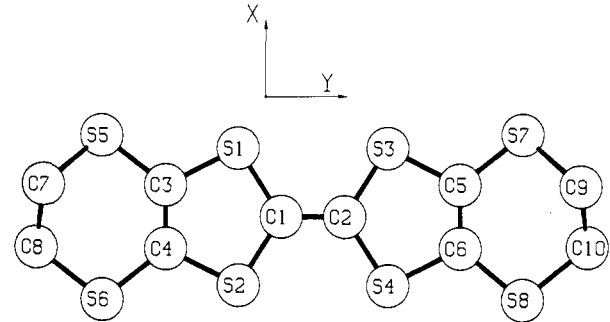


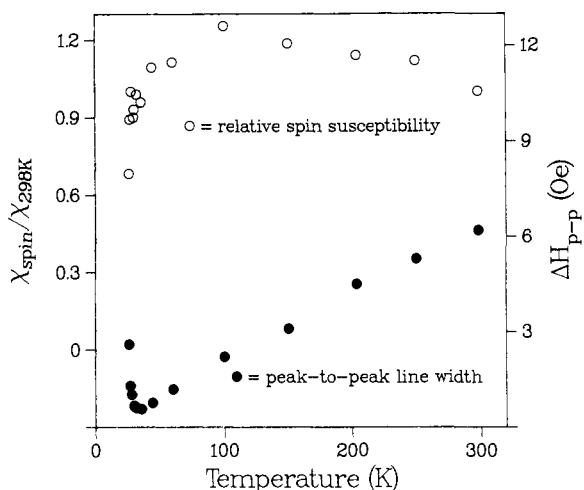
Figure 1. Electrical resistivity from 300 to 160 K showing semiconducting behavior: (A) β -(ET)₂AuCl₂, (B) β -(ET)₂ICl₂.

Table III. Intramolecular Distances (Å) and Angles (deg) for β -(ET) $_2$ AuCl $_2$ at 298 K/120 K^a


A. Distances (Å) for the ET Molecule and the AuCl $_2^-$ Anion			
S1-C1	1.739 (3)/1.740 (2)	S1-C3	1.750 (3)/1.748 (2)
S2-C1	1.742 (3)/1.744 (2)	S2-C4	1.754 (3)/1.756 (2)
S3-C2	1.740 (3)/1.746 (2)	S3-C5	1.752 (3)/1.754 (2)
S4-C2	1.738 (3)/1.741 (2)	S4-C6	1.750 (3)/1.753 (2)
S5-C3	1.744 (4)/1.749 (2)	S5-C7	1.810 (4)/1.815 (2)
S6-C4	1.749 (3)/1.747 (2)	S6-C8	1.818 (4)/1.825 (2)
S7-C5	1.754 (3)/1.751 (2)	S7-C9	1.811 (5)/1.812 (2)
S8-C6	1.743 (3)/1.747 (2)	S8-C10	1.799 (5)/1.812 (2)
C1-C2	1.366 (4)/1.367 (2)	C3-C4	1.344 (5)/1.361 (2)
C5-C6	1.344 (5)/1.355 (2)	C7-C8	1.493 (6)/1.513 (3)
C9-C10	1.475 (7)/1.518 (3)	Au-C1	2.269 (1)/2.272 (1)

B. Angles (deg) for the ET Molecule			
C1-S1-C3	95.3 (2)/95.3 (1)	C1-S2-C4	95.4 (2)/95.3 (1)
C2-S3-C5	95.3 (2)/95.5 (1)	C2-S4-C6	95.2 (2)/95.3 (1)
C3-S5-C7	98.0 (2)/98.0 (1)	C4-S6-C8	103.1 (2)/103.1 (1)
C5-S7-C9	99.5 (2)/99.2 (1)	C6-S8-C1	101.4 (2)/101.0 (1)
C2-C1-S1	122.6 (3)/122.5 (1)	C3-C4-S2	116.8 (3)/116.3 (1)
C2-C1-S2	122.3 (3)/122.1 (1)	C3-C4-S6	129.1 (3)/129.3 (1)
S1-C1-S2	115.1 (2)/115.4 (1)	S2-C4-S6	114.1 (2)/114.4 (1)
C1-C2-S3	122.5 (3)/122.1 (1)	C6-C5-S3	116.9 (2)/116.6 (1)
C1-C2-S4	122.3 (3)/122.7 (1)	C6-C5-S7	128.1 (3)/127.9 (1)
S3-C2-S4	115.2 (2)/115.2 (1)	S3-C5-S7	115.0 (2)/115.5 (1)
C4-C3-S1	117.3 (3)/117.4 (1)	C5-C6-S4	117.2 (3)/117.3 (1)
C4-C3-S5	126.7 (3)/126.3 (1)	C5-C6-S8	129.5 (3)/129.7 (1)
S1-C3-S5	116.0 (2)/116.2 (1)	S4-C6-S8	113.3 (2)/113.0 (1)
C8-C7-S5	113.1 (3)/112.3 (1)	C10-C9-S7	115.0 (4)/113.0 (1)
C7-C8-S6	114.9 (3)/114.2 (1)	C9-C10-S8	115.0 (3)/113.0 (1)

^a Estimated standard deviations are enclosed in parentheses.

**Figure 2.** Temperature dependence of the ESR signal showing the phase transition of β -(ET) $_2$ AuCl $_2$ at \sim 33 K. The spin susceptibilities (open circles) are normalized to the 298 K value; the peak-to-peak line widths (Oe) are represented by solid circles. The single crystal was oriented with the c^* axis nearly parallel to the static magnetic field.

temperature to 0.6 Oe at 33 K, at which point it rose abruptly as the temperature was lowered further. The relative spin susceptibility rose gradually with decreasing temperature from 298 to about 50 K, where it decreased steadily at first and then dropped sharply below about 33 K. Below about 33 K, the ESR line width

Table IV. Interdonor S...S Interaction Distances for β -(ET) $_2$ AuCl $_2$ and Other β -(ET) $_2$ X Salts at 298 K/120 K^a

contact	β -(ET) $_2$ AuCl $_2$ distance	β -(ET) $_2$ ICl $_2$ distance	β -(ET) $_2$ IBr $_2$ distance	β -(ET) $_2$ AuI $_2$ distance
A. Distances Less Than 4.0 Å along the a -Axis Directions				
S5...S6	3.429/3.398	3.454/3.421	3.572/3.551	3.563/3.515
S7...S8	3.443/3.418	3.445/3.416	3.560/3.510	3.568/3.517
S3...S8	3.555/3.526	3.536/3.504	3.652/3.593	3.598/3.524
S2...S5	3.560/3.520	3.542/3.507	3.559/3.514	3.569/3.516
B. Distances Less Than 4.0 Å along the b -Axis Directions				
S2...S2	3.690/3.585	3.697/3.609	3.944/3.841	3.912/3.829
S4...S6	3.748/3.672	3.707/3.642	3.754/3.655	3.693/3.606
S5...S7	3.934/3.810	3.935/3.829	3.593/3.498	3.674/3.589
C. Distances Less Than 4.0 Å along the $(-a-b)$ Direction				
S1...S4	3.715/3.655	3.648/3.596	3.772/3.730	3.745/3.699
S2...S3	3.748/3.687	3.727/3.678	3.748/3.723	3.736/3.685
S3...S4	3.765/3.727	3.833/3.803	3.795/3.730	3.808/3.735

^a Refer to Figure 3 for the unit cell vectors within the ab plane. The a -axis direction for all β -(ET) $_2$ X salts is nearly along the short in-plane axis of the ET molecule. Estimated standard deviations for the S...S distances are in the range ± 0.001 to ± 0.002 Å. The S...S distances along the stacking ($a + b$) direction are equal to or greater than 4.0 Å.

was very large. The g value for this ESR signal (calibrated with 0.1% strong pitch) was relatively constant in the range 298–44 K, with deviations of only ± 0.0002 from the mean value of 2.0038. Upon reaching the transition temperature, there was a noticeable increase in the g value from 2.0036 at 44 K to 2.0047 at 26 K.

The abrupt and simultaneous increase in the ESR line width and g value and the decrease in susceptibility of β -(ET) $_2$ AuCl $_2$ near 33 K closely resemble the ESR properties of β -(ET) $_2$ ICl $_2$ ¹⁰ and (TMTSF) $_2$ PF $_6$.²⁰⁻²² The (TMTSF) $_2$ PF $_6$ salt is metallic down to about 15 K at which temperature it undergoes a spin density wave transition. On the basis that its ΔH_{p-p} value decreases with decreasing temperature (above 22 K), the β -(ET) $_2$ ICl $_2$ salt was thought to be a metal.¹⁰ However, β -(ET) $_2$ ICl $_2$ and β -(ET) $_2$ AuCl $_2$ as well are not metallic as described in the previous section. Thus an ESR result for a salt in which its ΔH_{p-p} value decreases with decreasing temperature does not guarantee that the salt is metallic.

Chainlike Donor-Donor Network and Short H...Cl Contacts

The type I salts, β -(ET) $_2$ AuCl $_2$ and β -(ET) $_2$ ICl $_2$, are isostructural, even though the AuCl $_2^-$ anion, with a length of 8.1 Å, is ~ 0.6 Å shorter than ICl $_2^-$ (including the van der Waals radii sum, 3.6 Å, of the two exterior Cl atoms¹⁵). Such a variation in anion length is significant since, for the same reduction in anion length between IBr $_2^-$ (9.30 Å) and ICl $_2^-$ (8.72 Å), dramatic differences in the donor network motifs and electrical properties of their salts have been observed. Namely, β -(ET) $_2$ IBr $_2$ remains metallic and becomes superconducting at ambient pressure at about 2.8 K^{8,9} whereas β -(ET) $_2$ ICl $_2$ is semiconducting and undergoes a phase transition at 22 K.¹⁰ Therefore, β -(ET) $_2$ AuCl $_2$, which contains the shortest linear anion incorporated so far in a β -(ET) $_2$ X salt, represents a *new lower limit* for anion length or unit cell volume for a β -(ET) $_2$ X phase. As a consequence of having a shorter anion, β -(ET) $_2$ AuCl $_2$ has a more compact and dimerized ET molecule network than that in β -(ET) $_2$ ICl $_2$. Listed in Table IV are the S...S contacts less than 4.0 Å within the donor network in the ab plane [i.e., along the crystallographic a , b , and $(-a-b)$ directions] of type I salts, β -(ET) $_2$ AuCl $_2$ and β -(ET) $_2$ ICl $_2$, and type II salts, β -(ET) $_2$ IBr $_2$ and β -(ET) $_2$ AuI $_2$. The ET molecule networks and adjacent anion layers in the type I salt β -(ET) $_2$ AuCl $_2$ and the type II salt β -(ET) $_2$ IBr $_2$ are shown in Figure 3. It is noted that the four shortest S...S distances for the type I and type II β -(ET) $_2$ X salts are always along the a -axis direction (i.e., the interstack direction). The existence of these short S...S contacts

(20) Pedersen, H. J.; Scott, J. C.; Bechgaard, K. *Phys. Rev. B: Condens. Matter* **1981**, *24*, 5014. TMTSF is tetramethyltetraselenafulvalene.

(21) Mortensen, K.; Tomkiewicz, Y.; Schultz, T. D.; Engler, E. M. *Phys. Rev. Lett.* **1981**, *46*, 1234.

(22) Andrieux, A.; Jerome, D.; Bechgaard, K. *J. Phys. Lett.* **1981**, *42*, L87.

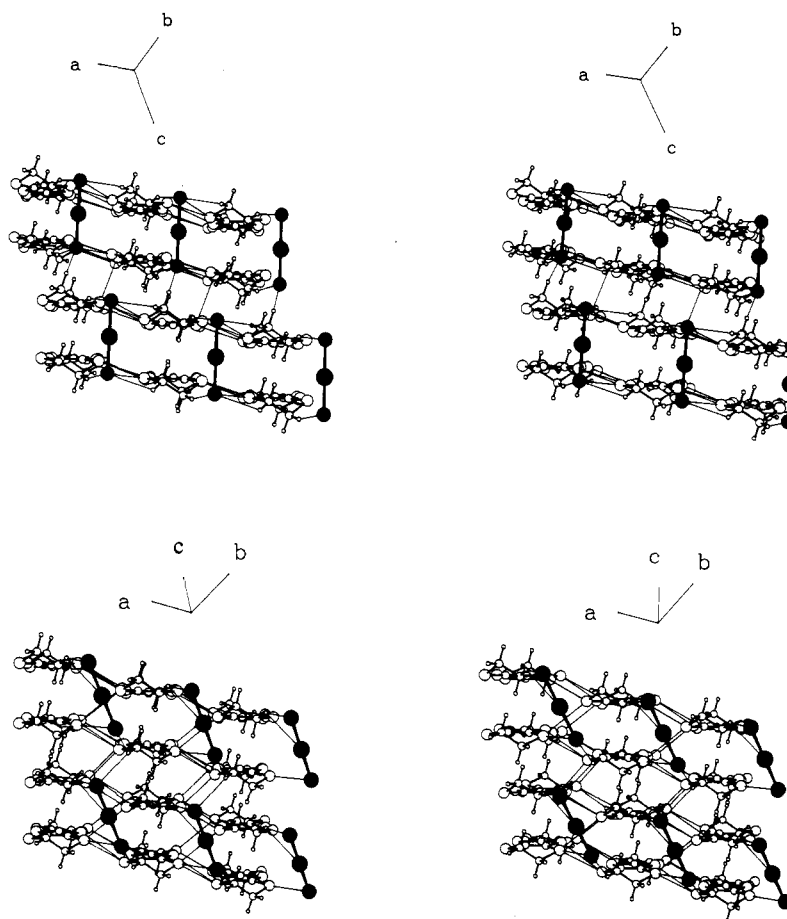


Figure 3. (Top) Stereoview of the ab -plane network of ET molecules (open thermal ellipsoids) and the nearby AuCl_2^- anions (shaded thermal ellipsoids) in the type I salt $\beta\text{-(ET)}_2\text{AuCl}_2$. van der Waals contact distances between the ET donor molecules and the AuCl_2^- anion are indicated by thin lines (see Tables IV–VI). (Bottom) Stereoview of the donor network and adjacent anion layer including van der Waals contacts (thin lines) in the type II salt $\beta\text{-(ET)}_2\text{IBr}_2$. Arbitrary thermal ellipsoids are used.

is possible because of the close side-by-side packing of the ET molecule chains within the networks. The large degree of dimerization of the ET molecules in type I salts allows for an anisotropic arrangement of S...S contacts within the ET network such that only those contact distances that are along the a axis are shorter than the van der Waals radii sum.¹⁵ In contrast, type II salts have S...S contacts that are shorter than the van der Waals radii sum in the b and $(-b-a)$ directions as well as the a -axis direction (see Figure 3). For all $\beta\text{-(ET)}_2\text{X}$ salts, the contraction of the a -axis S...S contact distances from 298 to 120 K is, on the average, only half that for S...S distances along any other direction within the ET molecule network (see Table IV). Thus, the contraction of nearest-neighbor interdonor spacings is anisotropic for all $\beta\text{-(ET)}_2\text{X}$ salts and is likely the result of crystal packing effects. This anisotropic contraction tends to further isolate the ET molecule dimers from each other in the type I $\beta\text{-(ET)}_2\text{X}$ salts, which are semiconducting and undergo phase transitions at low temperatures. Axial rotation photographs of the X-ray diffraction intensities about the a , b , c axes in the type I compound, $\beta\text{-(ET)}_2\text{ICl}_2$, at about 15 K, which is below the magnetic phase transition, show no evidence of superlattice formation.¹⁰ In summary, the dimerization of ET molecules in these types I materials is increased upon temperature lowering, but without any apparent crystallographic transition or lattice dimerization below the low temperature phase transition.

Table V shows the lengths of the anions X^- and the average distances of the a -axis S...S contacts for type I and type II $\beta\text{-(ET)}_2\text{X}$ salts. These average S...S distances decrease as the anion lengths decrease. As shown in Figure 3, the ET dimers of type I salts do not form a smooth ET molecule layer but protrude into the anion sheets to such an extent that the anions are greatly separated from each other. This is not the case for type II salts. The short hydrogen...terminal halogen and short terminal halo-

Table V. Anion Length Correlation Data for $\beta\text{-(ET)}_2\text{X}$ Salts

phase	anion	length ^a	S...S ^b
β	I_3^-	10.14 ^c	3.606
β	I_2Br^-	9.72 ^d	3.595
β	AuI_2^-	9.42 ^c	3.560
β	IBr_2^-	9.30 ^c	3.569
β' ^e	BrICl^-	9.01 ^d	3.495
β'	ICl_2^-	8.72 ^c	3.494
β'	AuCl_2^-	8.14 ^c	3.497

^a Anion length (\AA) includes van der Waals radii of outer atoms.

^b Average of the four shortest S...S contact distances (\AA) (see Table IVA and text). Largest esd of any component S...S value is ± 0.003 \AA .

^c The interatomic distances of this anion were computed from 120 K X-ray data. All other data from 298 K crystal structures. ^d Anion length of I-I-Br^- assumed to be intermediate to those of I_3^- and IBr_2^- ; anion length of Br-I-Cl^- assumed to be the average of IBr_2^- and ICl_2^- .

^e The β' phase refers to the type I salts, and the β phase refers to the type II salts.

gen...sulfur contact distances observed for type I and type II salts are listed in Table VI. These contact distances decrease as the size of the terminal-halogen atom decreases, which must originate from the fact that ET molecules are closely packed around each anion, X^- . Therefore, close-packing of ET molecules around anions, X^- , is a necessary structural feature for the correlation between the a -axis interdonor contacts and the anion length for $\beta\text{-(ET)}_2\text{X}$ materials.

Band Electronic Structure

Shown in Figure 4 is the band electronic structure of $\beta\text{-(ET)}_2\text{AuCl}_2$ calculated for its 120 K crystal structure in the same manner performed for $\beta\text{-(ET)}_2\text{ICl}_2$.¹⁰ The two bands result primarily from the HOMO of each ET molecule and are very similar in character to those calculated for $\beta\text{-(ET)}_2\text{ICl}_2$.¹⁰ With

Table VI. Donor–Anion Interaction Distances for Completely Ordered Type I and Type II β -(ET)₂X Salts at 120 K

contact	type I salts		type II salts			
	X ⁻ = AuCl ₂ ⁻ distance	X ⁻ = ICl ₂ ⁻ distance	β -(ET) ₂ IBr ₂		β -(ET) ₂ AuI ₂	
			contact	distance	contact	distance
A. Calculated H...Halogen Distances (Å) ^a						
Cl...H72	2.61	2.59	Br...H102	2.91	I...H102	3.03
Cl...H101	2.63	2.64	Br...H81	2.92	I...H81	3.13
Cl...H91	2.73	2.78	Br...H102'	2.93	I...H102'	3.24
Cl...H82	2.90	2.88	Br...H82	3.18	I...H82	3.39
Cl...H92	2.92	2.91	Br...H92	3.19	I...H92	3.27
					I...H71	3.20
B. Observed S...Halogen Distances (Å)						
Cl...S6	3.423	3.441	Br...S7	3.761	I...S7	3.832
Cl...S7	3.581	3.671	Br...S5	4.000	I...S5	4.057

^a For this comparison, only the donor–anion distances to the terminal halogen atoms that are nearly equal to or less than their associated van der Waals radii¹⁵ sums are given, namely: Cl–H 3.00 Å; Br–H 3.15 Å; I–H 3.35 Å; Cl–S 3.65 Å; Br–S 3.80 Å; I–S 4.00 Å. Estimated standard deviations for S...halogen distances are in the range ± 0.002 to ± 0.003 Å.

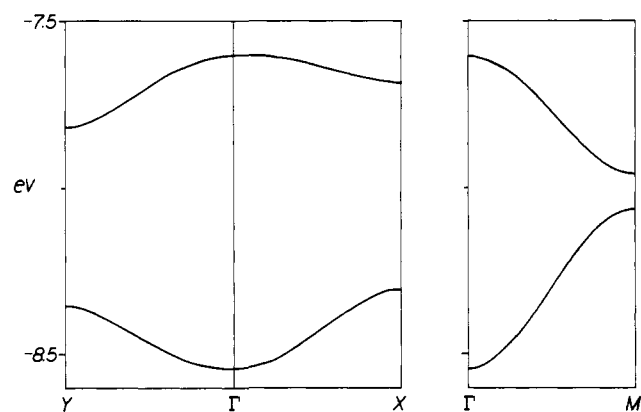
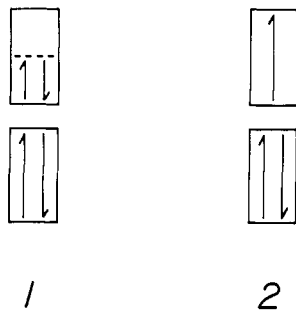


Figure 4. Dispersion relations for the two highest occupied bands of β -(ET)₂AuCl₂ at 120 K. Γ , X, Y, and M represent the wavevector points (0,0), ($a^*/2,0$), (0, $b^*/2$), and ($-a^*/2,b^*/2$), respectively, of the first Brillouin zone within the a^*b^* plane.

the formal oxidation of (ET)₂⁺ per unit cell, there are three electrons to fill the two bands so that the upper band is half-filled. This band shows a strong 1D character since it is almost dispersionless along $\Gamma \rightarrow X$. The $\Gamma \rightarrow X$ direction in reciprocal space corresponds to the a -axis direction in the real space in which short interdimer S...S contacts occur. The weak band dispersion along $\Gamma \rightarrow X$ results from the fact that the nature of overlap between ET molecule HOMOs along the a -axis direction is primarily π -type instead of σ -type. It was shown before that a σ -type overlap is more effective than a π -type overlap in giving rise to a strong band dispersion and is significant even though interdimer S...S contact distances are not smaller than 3.6 Å. Since β -(ET)₂AuCl₂ and β -(ET)₂ICl₂ are semiconducting even at room temperature, the upper band is not filled in a low-spin manner (see 1) to become metallic but in a high-spin manner (see 2) to become magnetic insulating.^{23,24} The electron-localized state 2 represents a case



in which every ET dimer unit is a cation radical center. The activation energy of ~ 0.1 eV observed for the electrical conduction of β -(ET)₂AuCl₂ and β -(ET)₂ICl₂ represents the energy required for an electron to hop from one dimer unit, (ET)₂⁺, to another. In contrast, the β -(ET)₂X salts with long, linear anions (i.e., type II salts with X⁻ = I₃⁻, I₂Br⁻, AuI₂⁻, IBr₂⁻) are 2D metals on the basis of both their electrical conductivities^{1,2,25–27} and the band electronic structures.^{13,14}

Summary and Concluding Remarks

The β -(ET)₂X materials which contain short (8.1–8.7 Å) linear anions, X⁻ described herein as type I salts, differ from those of type II salts, which have long (9.3–10.1 Å) linear anions, in two respects: (i) The donor molecule networks in type I salts are composed of weakly interacting chains of strongly dimerized ET molecules, in contrast to type II salts, which have strongly interacting chains of weakly dimerized ET molecules. The dimerized ET molecules in the donor networks of type I salts lead to their quasi-1D band electronic structures, as calculated here for β -(ET)₂AuCl₂. In contrast, type II salts are 2D metals that may become superconducting at low temperatures, depending upon the degree of molecular order. (ii) For the type I salts, the four shortest S...S contacts (3.40–3.56 Å) between ET molecules occur only in one direction (i.e., a -axis direction). The anisotropy of donor–donor interactions depends on the extent of dimerization of the ET molecules, which is greater for the type I salts. A direct correlation between anion length and the four shortest S...S distances is observed for β -(ET)₂X salts, viz., shorter S...S distances occur for shorter anion lengths. This correlation exists for both type I and type II salts because ET molecules are closely packed around each anion, X⁻, so that the type of donor–anion interactions that are present in the type II salts occur in the type I salts as well despite the dramatic changes in the ET molecule network. For type I salts to allow the anions to be close-packed by ET molecules, the dimerized ET molecule pairs protrude out of their donor networks. Finally, it appears that the β -(ET)₂X salts containing halide-based anions that are shorter than ICl₂⁻ and AuCl₂⁻ will likely have semiconducting or insulating electrical properties.

Acknowledgment. Work at Argonne National Laboratory is sponsored by the U.S. Department of Energy (DOE), Office of Basic Energy Sciences, Division of Materials Sciences, under Contract W-31-109-ENG-38. C.M.P. and B.A.A. are student research participants coordinated by the Argonne Division of Educational Programs from Immaculata College and Wittenberg University, respectively. Research at North Carolina State

(23) Jacobsen, C. S.; Williams, J. M.; Wang, H. H. *Solid State Commun.* **1985**, *54*, 937.

(24) Carlson, K. D.; Crabtree, G. W.; Choi, M.; Hall, L. N.; Copps, P. T.; Wang, H. H.; Emge, T. J.; Beno, M. A.; Williams, J. M. *Mol. Cryst. Liq. Cryst.* **1985**, *125*, 145.

(25) Tokumoto, M.; Bando, H.; Anzai, H.; Saito, G.; Murata, K.; Kajimura, K.; Ishiguro, T. *J. Phys. Soc. Jpn.* **1985**, *54*, 869.

(23) Whangbo, M.-H. *Acc. Chem. Res.* **1983**, *16*, 95.

(24) Whangbo, M.-H. *Crystal Chemistry and Properties of Materials with Quasi One-Dimensional Structures*; Rouxel, J., Ed.; Reidel: Dordrecht, 1986.

University was in part supported by DOE, Office of Basic Energy Sciences, Division of Material Sciences, under Grant DE-FG05-86ER45259. The authors express their appreciation for computing time on the ER-Cray X-MP computer, made available by the DOE.

Registry No. β -(ET)₂AuCl₂, 106343-40-2.

Supplementary Material Available: Tables of the refined anisotropic thermal parameters for all non-hydrogen atoms at 298 K and 120 K and the calculated H-atom fractional coordinates for β -(ET)₂AuCl₂ at 298 and 120 K (3 pages); listing of observed and calculated structure factors for β -(ET)₂AuCl₂ at 298 K and 120 K (28 pages). Ordering information is given on any current masthead page.

Tungsten and Molybdenum 2-Oxaallyl (η^1 -(C)-Enolate) Complexes: Functional Group Transformations, Photochemical Aldol Reactions, and Alkyne/CO Migratory Insertion Reactions

Elizabeth R. Burkhardt, Jeffrey J. Doney, Robert G. Bergman,* and Clayton H. Heathcock*

Contribution from the Department of Chemistry, University of California, Berkeley, California 94720. Received August 25, 1986

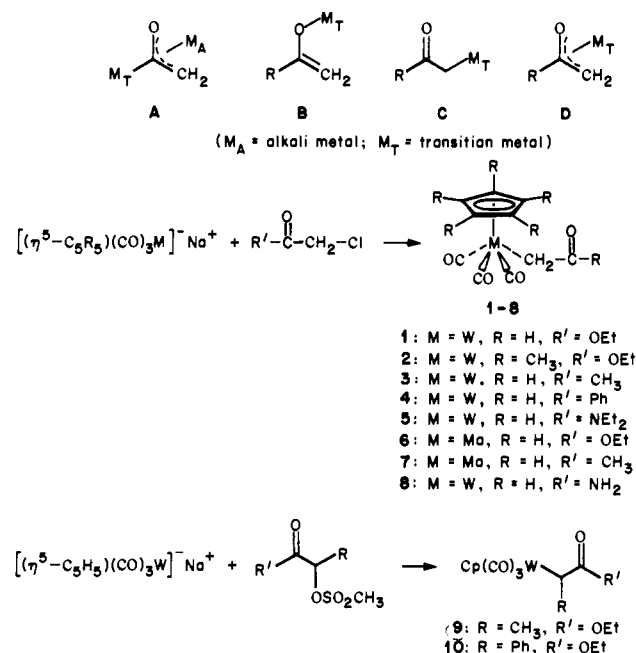
Abstract: Carbon bound tungsten and molybdenum 2-oxaalkyl (η^1 -enolate) complexes **1–8** can be prepared easily by reaction of $C_5R_5(CO)_3M^- Na^+$ ($R = H, CH_3; M = W, Mo$) with α -chloro esters, ketones, and amides. Secondary tungsten enolates **9** and **10** were successfully prepared by using α -methanesulfonyl esters. Organic carbonyl functional group transformations were carried out on $Cp(CO)_3W(CH_2CO_2Et)$ without M–C bond cleavage, leading to several new enolates including the novel organometallic acid chloride $Cp(CO)_3WCH_2COCl$ (**13**). Loss of CO from carbon bound enolates generated η^3 -oxaallyl complexes **15–21**. These are stable in solution, but only one, $Cp(CO)_2WCH_2CONEt_2$ (**18**), can be isolated. The tungsten η^3 -oxaallyl complexes undergo reaction with CO to regenerate the parent complexes and substitution reactions with various ligands (PPh₃, CH₃CN, C₅H₅N, Ph₂PCH₂PPh₂, and PhC \equiv CH) to give new isolable substituted η^1 -enolate complexes. The primary tungsten enolates undergo photochemical aldol condensation with aldehydes to give aldolates **31, 33, 34**, and **36** and give combined CO/alkyne insertion products **44** and **46** with alkynes. Evidence is presented supporting the intermediacy of the η^3 -oxaallyl complexes in the ligand substitution, aldol, and alkyne insertion reactions. In addition, crystal structures of the following complexes have been obtained: η^1 -enolate $Cp(CO)_3WCH_2CO_2Et$ (**1**), η^3 -oxaallyl $Cp(CO)_2WCH_2CONEt_2$ (**18**), bisalkyne complex $Cp(PhC\equiv CH)_2WCH_2CO_2Et$ (**49**), oxo/alkyne complex $Cp(PhC\equiv CH)(O)WCH_2CO_2Et$ (**50**), and CO/alkyne insertion product **44**.

The exploitation of highly ordered transition states in organic reactions to obtain predictable reactivity is an important goal of organic chemistry. The specific relative orientation of organic ligands located in the coordination sites of transition-metal centers provides a method for generating such ordered transition states, and this technique has been used increasingly in recent years to control stereochemistry in organic reactions.¹

Partly because of the utility of the aldol reaction in constructing hydroxylated carbon chains, extensive studies have been carried out aimed at developing methods for executing this transformation with a high degree of stereoselectivity.¹ The techniques employed normally utilize a chiral group attached to the enolate reactant; transfer of chirality from the enolate to the newly formed stereocenter can then be achieved in some cases with very high degrees of selectivity. Many types of chiral enolates have been utilized, including those with organic chiral auxiliaries attached to the carbonyl group of the enolate,² as well as those with optically active ligands bound to main group metals coordinated to the enolate oxygen atoms.³

One group of enolates whose propensity to engage in aldol reaction has been little examined is the group of so-called "late" transition-metal enolates (i.e., those utilizing transition metals lying to the right of group V (Group 5, see ref 73) in the periodic table)

Scheme I



(1) Heathcock, C. H. *Asymmetric Synthesis*; Morrison, J. D., Ed.; Academic Press: New York, 1983; Vol. 3.

(2) (a) Heathcock, C. H. *Asymmetric Reactions and Processes in Chemistry*; Eliel, E. L., Otsuka, S., Eds.; American Chemical Society: Washington, DC, 1982. (b) Evans, D. A. *Asymmetric Synthesis*; Morrison, J. D., Ed.; Academic Press: New York, 1983; Vol. 3.

(3) Iwasawa, N.; Mukaiyama, T. *Chem. Lett.* **1982**, 1441.

in which the metal is bound to the potentially reactive carbon atom (type C in Scheme I). None of the complexes in this class have been shown to engage in aldol chemistry. In this paper we describe